



Hardware article

High-performance wide-band open-source system for acoustic stimulation

Artur Silva ^{a,*}, Filipe Carvalho ^{a,b,1}, Bruno F. Cruz ^{a,c,d}

^a Champalimaud Research, Champalimaud Foundation, Av. Brasília, Lisbon, Portugal

^b Open Ephys Production Site, Rua Afonso Praça 30, Lisbon, Portugal

^c NeuroGEARS Ltd, 31 Oval Road, London, United Kingdom

^d Allen Institute for Neural Dynamics, 615 Westlake Ave N, Seattle, United States



ARTICLE INFO

Keywords:

Audio

Sound card

Audio amplifier

Auditory stimuli

Acoustic stimulation

ABSTRACT

The design and characterization of a low-cost, open-source auditory delivery system to deliver high performance auditory stimuli is presented. The system includes a high-fidelity sound card and audio amplifier devices with low-latency and wide bandwidth targeted for behavioral neuroscience research. The characterization of the individual devices and the entire system is performed, providing a thorough audio characterization data for varying frequencies and sound levels. The system implements the open-source Harp protocol, enabling the hardware timestamping of devices and seamless synchronization with other Harp devices.

Specifications table

Hardware Name	Harp Sound Card, Harp Audio Amplifier
Subject Area	•Electronic Engineering •Neuroscience
Hardware Type	•High Performance Audio System
Closest Commercial Analog	High fidelity sound cards and audio amplifiers
Open Source License	The TAPR Open Hardware License.
Cost of Hardware	396€
Source File Repository	http://doi.org/10.17632/xxzcfw3n4.1

1. Hardware in context

Experimental behavior neuroscience relies on the ability to observe and measure the environment the animal lives in, as well as manipulate it. For most animals, and especially mammals, hearing is a critical sense. Among others, sound pressure levels can be used to provide critical information about where to forage or hunt [1,2], detect and avoid threats [3], navigate [4], and even communication with conspecifics [5]. While much can be learned from recording auditory features from the environment, it is often also necessary to “close the loop” by generating experimentally controlled stimuli [6].

Sound can be defined as a longitudinal pressure wave that travels in both space and time through a physical medium. An amplitude and single frequency characterize pure tone waveforms. As one might expect, the domain of these features in which

* Corresponding author.

E-mail addresses: artur.silva@research.fchampalimaud.org (A. Silva), filipe@oeps.tech (F. Carvalho).

¹ The two authors contributed equally to this work.

<https://doi.org/10.1016/j.ohx.2024.e00555>

Received 7 March 2024; Received in revised form 26 June 2024; Accepted 29 June 2024

Available online 4 July 2024

2468-0672/© 2024 The Author(s). Published by Elsevier Ltd. This is an open access article under the CC BY license (<http://creativecommons.org/licenses/by/4.0/>).

animals can sense and produce sound partially defines their Umwelt [7] and is distinct across species. For instance, while human hearing is sensitive to frequencies of 30 Hz–20 kHz, mice expand the higher range to more than 85 kHz [8].

Unfortunately, devices capable of generating high-quality and experimentally controlled audio stimuli across a large section of this rich feature space are not widely available. Consumer-grade high-fidelity audio cards and amplifiers, while generally accessible and easy to use, are designed to operate within the human auditory domain (both intensity and frequency), a rather narrow band when compared to the space available to other species, and rarely include ways to externally synchronize and trigger the delivery of auditory stimuli, with timing benchmarks highly dependent on the audio drivers used [9,10].

Open source Linux-based architectures optimized for real-time embedded audio can provide low latency audio [11,12]. Examples include Elk Audio OS, which is optimized for low-latency and high-performance audio and sensor processing [13], BeagleRT, an environment for low-latency processing of audio and sensor data [14] and a multichannel, low-latency embedded Linux audio system [15]. Additionally, there are other open-source bespoke solutions for auditory sound generation, such as the open-source stimulation system for auditory EEG experiments [9], and the high-resolution audio device for Bpod system, which is targeted for rodent behavior measurement in multi-trial experiments [16]. Both of the aforementioned audio solutions support widely available hardware single board computers (SBCs), such as the Raspberry Pi [9,11,13] and BeagleBone Black platform [14,15]. To provide audio capabilities, commercially available HiFi Berry shields [9,11,13,16] and custom shields [13–15] with audio DAC implementations are used to interface with the SBCs. Despite the availability of these open-source solutions, the design files for the audio circuits of commercially available add-on shields are not available and there is a lack of comprehensive audio performance characterization (with the exception of [15,16]). More importantly, none of the systems offer end-to-end audio path characterization up to the audio amplifier and speaker element. This means that apart from latency measurements, the quality metrics of these systems are partially unknown, leaving a gap of uncertainty regarding the effective sound quality that is presented. For example, when the DAC is characterized as standalone, it does not guarantee that the output signal maintains the same performance specifications. Additional distortion can be introduced by the amplification or the speaker load, significantly affecting the signal. In the case of pure tone generation, the sound may be accompanied by additional harmonics, potentially compromising high-fidelity sound delivery.

High-end commercial solutions, like those provided by Tucker-Davis Technologies (TDT), can generate high-precision audio stimuli suited for neuroscience experiments with end-to-end audio characterization [17–19] but due to their prohibitive costs have seen relatively low adoption by the experimental neuroscience community.

To meet these needs, a complete end-to-end open-source auditory stimuli delivery system was designed to provide a cost-effective open-source alternative to commercial solutions while delivering low distortion and high-performance sound metrics. It is comprised of a sound card device equipped with a high-precision DAC and audio amplifier, ensuring a wide-bandwidth, low-latency, audio delivery system.

The flexibility of the system provides easy integration with other existing setups. At the firmware level, by implementing the Harp protocol [20] through a USB communication layer, the device can be easily controlled via Bonsai [21], or a provided graphical user interface (GUI). The former integration is especially relevant since it allows users to leverage already existing online processing tools (e.g. digital signal processing), control logic, and other third-party hardware (e.g. cameras, microphones, and displays), in a visual programming language environment. Adopting the Harp protocol also enables precise timestamping and synchronization with other Harp devices, allowing for scalable and robust experimental data collection pipelines. Alternatively, the device can also be pre-programmed via the aforementioned GUI to be triggered through simple TTL control logic provided by an external device/microcontroller, compatible with other existing hardware ecosystems (e.g. BPOD (Sanworks), PyControl [22] or other commercially available hardware).

Finally, despite previous solutions providing solutions to some of the individual problems phrased previously, we provide not only designs for an end-to-end solution (i.e. from DAC to speaker) but also report critical specifications benchmarks. While such a characterization is essential for behavior experimental design and validation, its acquisition might require dedicated lab equipment generally not available in neuroscience laboratories.

2. Hardware description

The proposed hardware system for acoustic stimulation provides an end-to-end solution. It comprises a custom-designed stereo sound card device responsible for generating high-performance analog audio signals and a low-distortion audio amplifier device for driving speakers. Both devices support wide-frequency bandwidth audio signals up to 80 kHz with a low distortion rate.

Sound waveforms can be pre-loaded in the internal memory of the sound card device, enabling low-latency sound delivery. The device also implements a high-fidelity sine-wave function generator that may be used to deliver pure tones without the need to upload a custom waveform.

An external trigger can be used to start the pre-stored sound waveform, with sub-millisecond latency, or triggered through software. In both scenarios the stimuli onset is timestamped by the microcontroller, providing the user with the real-time occurrence of this event at a resolution of 32 μ s).

At the time of this manuscript, the total cost for the electronic components, printed circuit boards (PCBs), and, power supplies is 396€ (242€ sound card, 154€ audio amplifier).

The proposed system fulfills the requirements for most auditory research experiments, with the following characteristics:

- Low-cost and open-source sound system
- Sub millisecond sound stimuli latency delivery
- 192 kHz, 24 bits sound card digital-to-analog converter

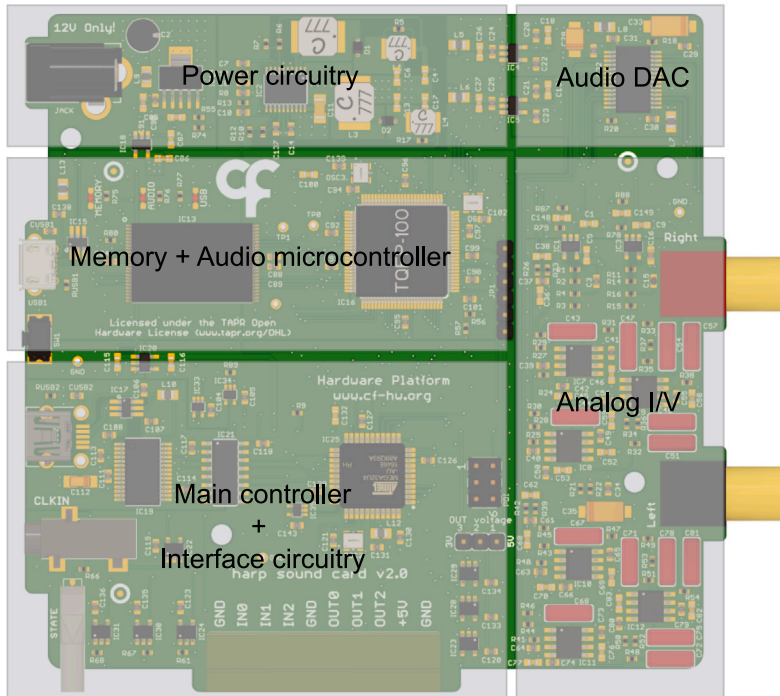


Fig. 1. PCB rendering of the sound card depicting the main circuit blocks.

- Wide frequency bandwidth system up to 80 kHz
- Low harmonic distortion
- Capable of driving speakers up to 4 W
- Compatibly with the Harp protocol, including clock synchronization between Harp devices

2.1. Sound card device

The sound card device is the core component of the system. It is responsible for storing and converting the digitized sound waves into high-resolution, low-distortion, and wide-band analog signals. The sound card device is composed of the power circuitry, main microcontroller and auxiliary circuitry, flash memory, audio microcontroller, audio digital-to-analog converter (DAC), and analog I/V (current-to-voltage) converter (Fig. 1).

A 12 V power supply is used to power the sound card. A ± 15 V step-up DC-DC followed by low-noise, low-dropout regulators are used to feed the analog I/V converter, providing a low noise and low ripple power supply to the analog circuitry. Independent analog and digital low dropout regulators are used for the audio DAC. For the digital section of the board (microcontrollers, memory, and auxiliary circuitry), a 5 V low-noise, fast transient-low dropout out regulator is used in series with additional 3.3 V low dropout regulators as points-of-load for different circuit parts. Given the large power dissipation of this fast-transient regulator, it is strongly recommended to attach a heat sink to the integrated circuit.

The circuit block of the main microcontroller is responsible for the USB communication (FT232RL, FTDI), Harp clock synchronization protocol, implementation of the Harp communication protocol [20], control of the digital I/O (input/output) interface, and serial communication with the audio microcontroller. The Harp sound card is fully compatible with the Harp family of devices, enabling a seamless clock synchronization between devices guaranteeing that events from multiple Harp boards are consistently aligned.

To minimize sound latency, waveforms are stored in flash memory through a dedicated micro-USB port. The system allows sound waveforms to be loaded into the memory without disrupting potentially playing waveforms. The audio microcontroller communicates with the flash memory via a parallel bus and interfaces with the DAC audio through inter-IC sound (I2S) serial bus interface. It executes all the audio-related processing functions according to the commands received by the main controller. A reset button is available to reset the 32-bit internal processor.

The DAC audio used (AD1955, Analog Devices) was chosen because of its high-performance stereo audio digital-to-analog converter with a 24-bit data resolution and a sample rate of up to 192 kHz. This DAC receives an I2S input and converts it into a differential current output signal using a multi-bit Sigma-Delta modulator. The conversion of the differential current from the DAC converter is done in two stages. The initial stage consists of an active op-amp current-to-voltage converter, which is used to convert

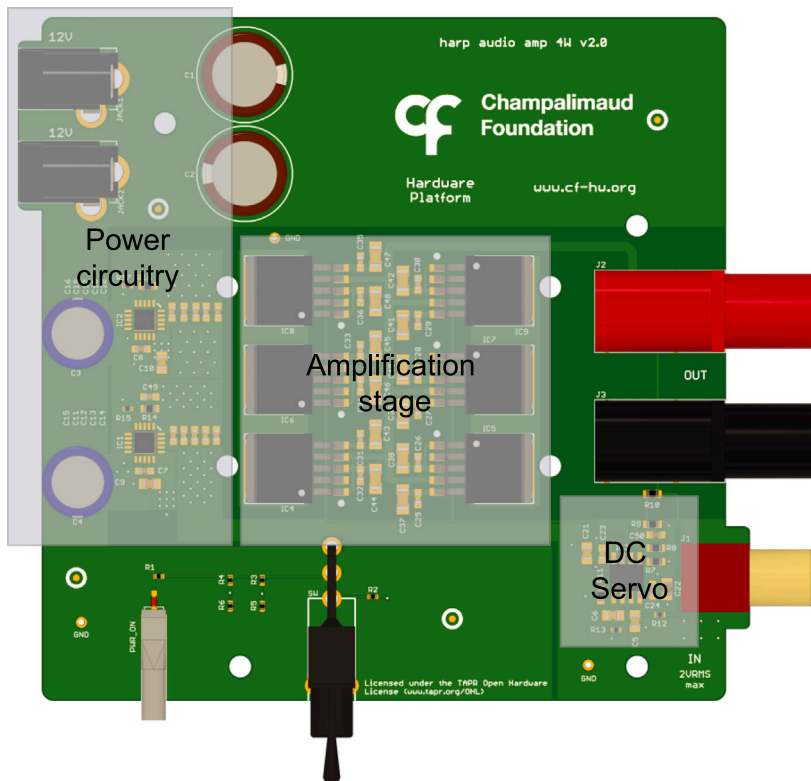


Fig. 2. PCB rendering of the audio amplifier board depicting the main circuit blocks.

each of the DAC current outputs to an analog signal. Subsequently, the I/V conversion is followed by a differential-to-single-ended buffer and low pass filter (with a cutoff frequency of 75 kHz at -3 dB), both implemented using op-amps. The sound card output voltage range is 2 V RMS.

The analog circuit block was designed to minimize noise and signal distortion, necessitating a careful choice of components. Operational amplifiers (OPA228UA, Texas Instruments) are used due to their combination of low noise and wide bandwidth operation. In the signal path, metal film chip resistors with high tolerance ($\leq 0.1\%$) and low-temperature coefficient (≤ 25 ppm), along with polypropylene film capacitors are chosen to ensure high signal generation precision and low distortion.

The sound card device has two RCA audio outputs to enable stereo audio output. The output amplitude is the typical audio line voltage, where full scale corresponds to 6 dBV (2 V RMS, 0 dBFS).

Four LEDs provide status information. The green LED will blink under the following conditions:

- Every 2 s during communication with a Harp-protocol host (e.g. Bonsai)
- Every 4 s when in standby mode
- Every 100 ms in the event of a catastrophic firmware error (occurs when the execution time of a specific function exceeds the maximum allowed time, potentially indicating a hardware failure or a firmware bug that the device cannot recover from, without manual intervention)

The three red LEDs will provide the following information:

- Memory LED will be on when accessing the memory
- Audio LED will turn on while generating audio
- USB LED will turn ON during USB communication or when USB communication is not available

2.2. Audio amplifier device

The sound card cannot provide a high current to the output load. Hence, to drive speakers, an audio amplifier board was designed. This board can output up to 4 W of power while maintaining a low signal distortion with a flat and wide frequency bandwidth.

The primary components of the audio amplifier device consist of three key blocks: the power supply regulators and decoupling capacitors, the amplification stage, and the DC servo circuitry (Fig. 2).

The power supply block includes two 12 V power supply connectors to generate a positive and negative voltage. This is achieved by using AC/DC power adaptors with floating outputs arranged in an anti-series configuration on the board. In this configuration, the positive terminal of the top power jack is used as the +12 V supply and the negative terminal of the power jack is used as

Table 1
Design files list.

Design filename	File type	Open source license	Location of the file
audio amplifier v2.0.brd	Eagle layout file	The TAPR Open Hardware License	https://doi.org/10.17632/xxzcffw3n4.1
audio amplifier v2.0.sch	Eagle schematic file	The TAPR Open Hardware License	https://doi.org/10.17632/xxzcffw3n4.1
audio amplifier BOM v2.0.xlsx	Excel BOM file	The TAPR Open Hardware License	https://doi.org/10.17632/xxzcffw3n4.1
sound card v2.2.brd	Eagle layout file	The TAPR Open Hardware License	https://doi.org/10.17632/xxzcffw3n4.1
sound card v2.2.sch	Eagle schematic file	The TAPR Open Hardware License	https://doi.org/10.17632/xxzcffw3n4.1
sound card BOM v2.2.xlsx	Excel BOM file	The TAPR Open Hardware License	https://doi.org/10.17632/xxzcffw3n4.1
soundcard source files v2.2.zip - Firmware.ATXMEGA	Firmware for the 8 bit microcontroller	MIT License	https://doi.org/10.17632/xxzcffw3n4.1
soundcard source files v2.2.zip - Firmware.PIC32	Firmware for the 32 bit microcontroller	MIT License	https://doi.org/10.17632/xxzcffw3n4.1

the -12 V supply voltage. The ground is connected to the remaining terminals of the power jacks. Low dropout regulators with low-output-noise and high-power supply ripple rejection are employed to supply the amplification and servo stages.

To achieve low noise and distortion, a composite configuration was implemented. Ultra-low distortion and low noise operational amplifier (LME49720, Texas Instruments) is used, followed by a high current buffer (LME49600, Texas Instruments) operating within the feedback loop of the operational amplifier. To further increase drive current capacity, several buffers are connected in parallel. Each buffer can drive a maximum current of up to ± 250 mA. Since the total noise and harmonic distortion of the buffer increase with the output power, the number of buffers employed is determined to ensure sufficient current headroom, thus keeping the distortion low.

A DC servo, consisting of an operational amplifier, compensates for the DC voltage offset in the feedback path and is implemented with a high pass filter pole set at 0.33 Hz. The role of the servo is not only to prevent a DC audio signal from being applied to the input of the amplifier device but also to remove small values of DC offset. The correction range of the offset is a function of the output voltage swing.

The amplifier is configured to operate at unity gain. Output power is specified according to the load, i.e., the impedance of the speaker that is used. For an 8Ω load, the amplifier can deliver up to 4 W, whereas with a 4Ω load, it can reach a maximum of 2 W (the maximum power at 4 W is limited by the current drive capacity of the amplifier, which requires a current higher than 1 A for lower loads).

In the context of the proposed audio system, given the amplifier unitary gain and the sound card maximum output voltage of 2 V RMS, the maximum output power produced is 0.5 and 1 W, at 8 and 4Ω , respectively.

3. Design files

3.1. Design files summary

The design files available in the repository are listed in [Table 1](#) and described below:

- audio amplifier v2.0.brd - Eagle file with the PCB layout of the audio amplifier board.
- audio amplifier v2.0.sch - Eagle file with the schematic of the audio amplifier board.
- audio amplifier BOM v2.0.xlsx - Bill of materials for the audio amplifier board, containing all the components to be assembled onto the PCB.
- sound card v2.2.brd - Eagle file with the PCB layout of the sound card.
- sound card v2.2.sch - Eagle file with the schematic of the sound card.
- sound card BOM v2.2.xlsx - Bill of materials for the sound card, containing all the - components to be assembled onto the PCB.
- Firmware.ATXMEGA - Folder with the firmware for the 8-bit processor (ATXmega128A1U, Microchip).
- Firmware.PIC32 - Folder with the firmware for the audio 32-bit processor (MZ2048EFM, Microchip).

A live version of the repository can be found here: <https://github.com/harp-tech/device.soundcard> and <https://github.com/harp-tech/peripheral.audioamp>.

4. Bill of materials

The bill of materials for both the sound and audio amplifier boards is available in the repository (<http://dx.doi.org/10.17632/xxzcffw3n4.1>). At the time of this manuscript, the printed circuit boards, produced in batches of 5 at SeedStudio, have a per-board cost of 22€ for the sound card and 19€ for the amplifier, with a total cost of 396€ for both boards. This total includes the electronic components, power supplies, cables, and PCBs, with a breakdown of 242€ for the sound card and 154€ for the audio amplifier.

5. Building instructions

A fully functional sound delivery system relies on the proper assembly of all the electronic components and the programming of the respective microcontrollers, as described below:

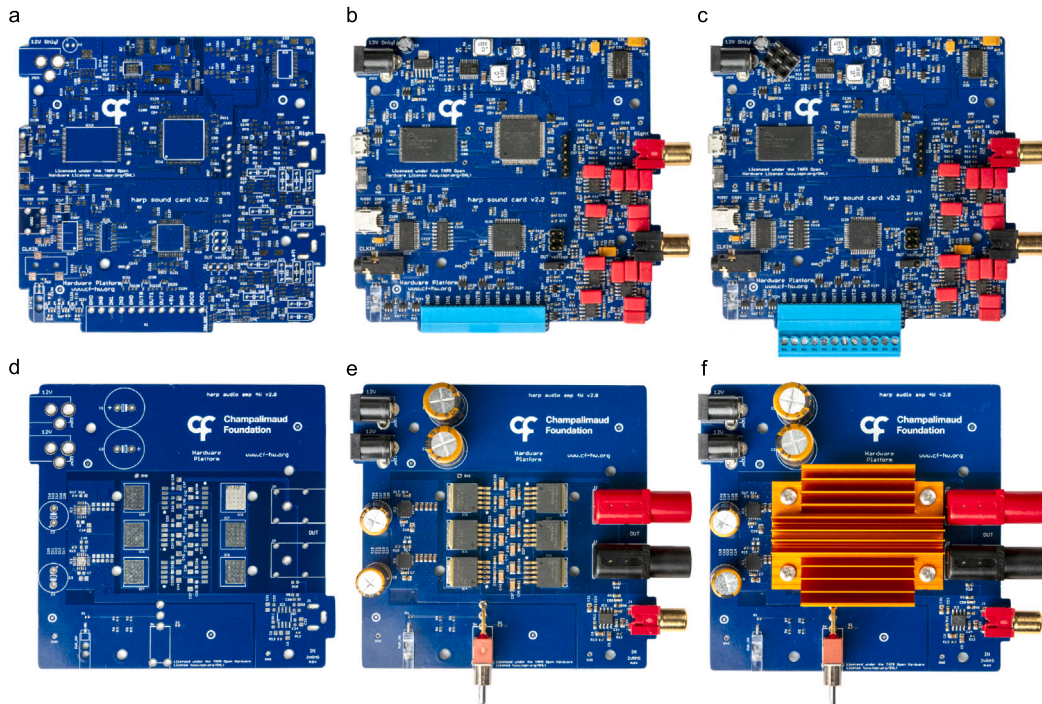


Fig. 3. Top side view of the PCBs. a, Harp sound card PCB. b, Harp sound card assembled. c, Harp sound card fully assembled with heatsink. d, Harp audio amplifier PCB. e, Harp audio amplifier assembled. f, Harp audio amplifier fully assembled with heatsink.

5.1. Printed circuit board assembly

The circuit schematic and the layout of the proposed devices were designed using the computer-aided design (CAD) software EAGLE. Users can use this software design files or the provided Gerber files to produce the PCBs. All CAD files for the device's boards, along with the respective bill of materials and technical files required for the assembly of the boards are available in the repository (<http://dx.doi.org/10.17632/xxzcfw3n4.1>).

The construction of this system requires the soldering of surface mount device (SMD) and through-hole (TH) components onto their respective PCBs (Fig. 3). Users may choose to assemble the boards themselves using hand or reflow soldering methods, provided they are comfortable with the process. Alternatively, the assembly can be outsourced to a third-party manufacturer capable of producing the PCBs, supplying the necessary components, and executing the complete assembly of the boards (e.g., PCBWay, Seeded Studio). The latter option is particularly recommended for the sound card device due to its numerous components.

5.2. Microcontroller programming

The sound card device requires firmware to be loaded into both microcontrollers. For each microcontroller a bootloader firmware was developed to enable subsequent firmware upgrades through the mini USB port eliminating the need for a dedicated programmer.

Therefore, it is necessary to load the respective bootloaders into the microcontrollers before uploading the firmware. The AVR XMEGA microcontroller requires the Microchip Studio IDE with an Atmel-ICE programmer or equivalent, whereas the PIC32 microcontroller uses the MPLAB IDE with a PIC32 programmer (e.g. PICKIT 3, Microchip) to load the respective bootloaders into the microcontrollers. The firmware can then be loaded using a dedicated Harp application - https://bitbucket.org/fchampallimaud/downloads/downloads/Harp_Convert_To_CSV_v1.8.3.zip.

Thus, to program the microcontroller the user needs to:

- Connect the Atmel-ICE programmer to the PDI connector in the sound card device
- Load the respective bootloader
- Connect the PIC32 programmer to the JP1 connector in the sound card device
- Load the respective bootloader
- Open the Convert to CSV application and write bootloader under List box on the Options tab
- Select the correspondent COM port and then select the firmware to be loaded for both microcontroller

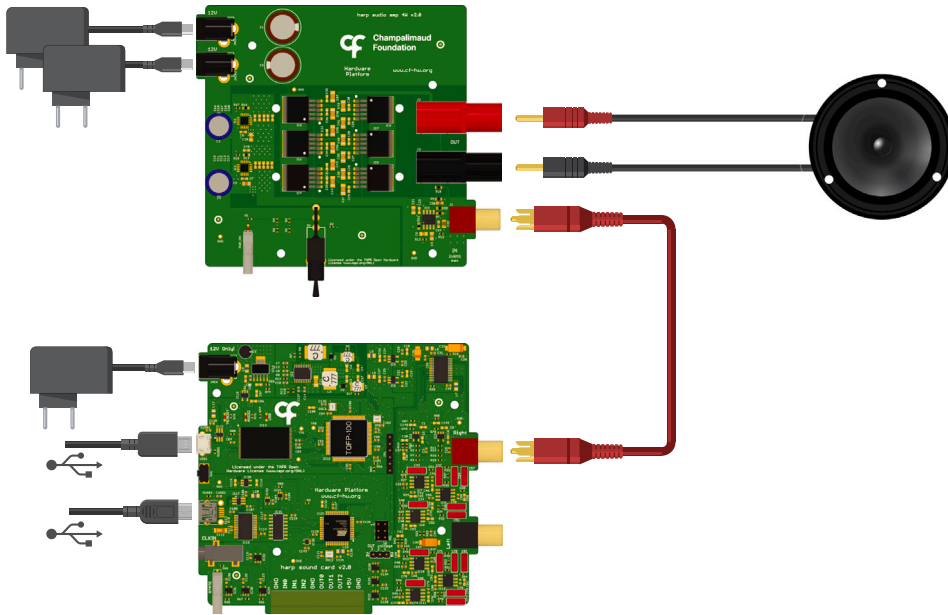


Fig. 4. Connection diagram of proposed system – sound card device connected to the audio amplifier device where a speaker is attached.

6. Operation instructions

6.1. Application example

To set up the hereto-introduced audio system (Fig. 4), the initial step involves the connection of one of the sound card outputs (RCA connectors) to the amplifier input (also equipped with an RCA connector). This is the case when using a single amplification channel. A speaker can then be connected to the 4 mm banana connector outputs of the amplifier. Under no circumstance should the audio card be used to directly drive high-resistance elements like speakers.

For the power supply, three 12 V adaptors are required: two for the amplifier and one for the sound card device. It is also necessary to switch ON the power button located on the amplifier board.

A mini- and a micro-USB cable connected to a computer are needed to enable control and upload sounds to the sound card.

Finally, drivers for both USB controllers need to be installed. Instructions for installing these drivers can be found in the repository (<http://dx.doi.org/10.17632/xxzcfw3n4.1>).

6.2. Sound card audio waveforms

The onboard sound card memory is partitioned into 32 indices (zero-indexed). The indexes from 2 to 31 are available for storing sounds, and each one of the sound indexes can store a sound file up to 8 megabytes (which corresponds to 2 million samples). An 8-MB file encodes waveforms of approximately 10.922 s at a 96 kHz sample rate, or 5.461 s at a 192 kHz sample rate (each sound sample is encoded as a 32-bit integer, although only the most significant 24 bits are used during sound reproduction). The internal memory is non-volatile and thus persists through power cycles. Example Python and Matlab scripts to generate valid waveforms are provided in the device's repository. Users can upload waveforms via the provided GUI by connecting the micro-USB cable to the sound card device, or through Bonsai.

6.3. Graphical user interface (GUI)

A graphical user interface was developed as an intuitive and easy-to-use interface to generate and upload sound files directly onto the sound card device, without the necessity for coding or the use of additional tools for sound generation (Fig. 5). This GUI was created using the graphical programming environment LabVIEW.

The GUI enables the generation of pure tones with configurable frequency, duration, and amplitude for each sound card channel, as well as the generation of uniform or Gaussian white noise, with adjustable time duration and amplitude that can be loaded directly into the sound card memory. Alternatively, the GUI provides the option to open and load an external waveform (WAV or binary files) onto the board.

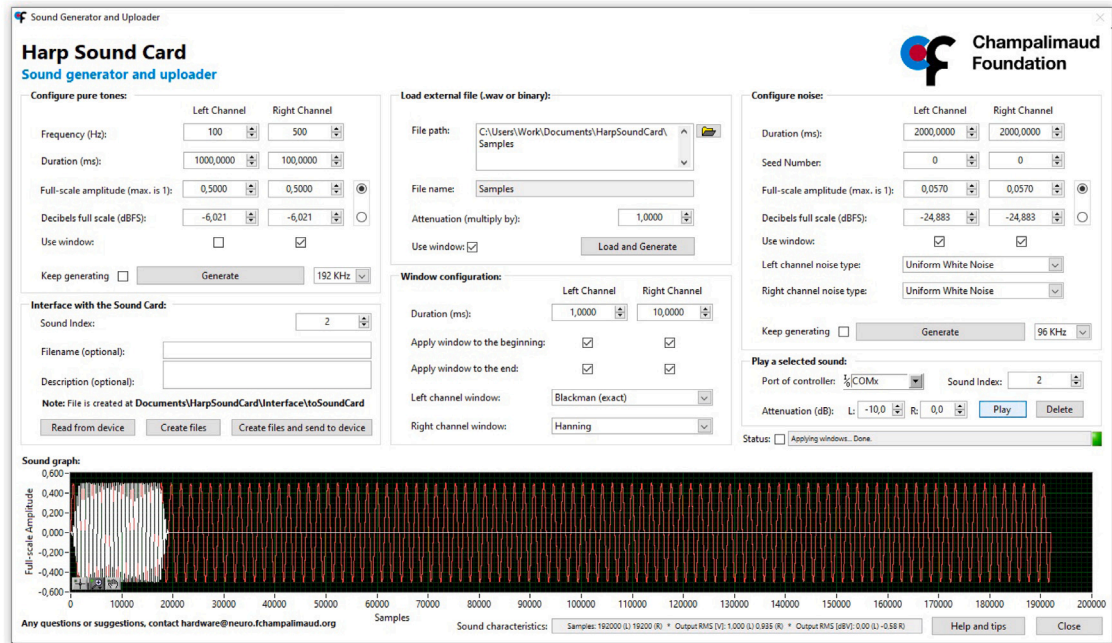


Fig. 5. Graphical user interface screenshot.

Whether creating a pure tone, noise or uploading an existing waveform file, users can apply a window to both of these signals (Hanning, Hamming or Blackman), with a configurable duration at the beginning, end, or both, during the generation process.

The generated signals can be previewed in the GUI in a time domain plot, depicting an amplitude versus samples, with zooming capabilities.

After the sound is generated, the user has the option to create a binary file compatible with the sound card device, which can be loaded into a specific sound index, along with an optional filename and description metadata.

6.4. Device interface

Various control strategies can be applied to generate sounds in the sound card device, allowing the users to select the one that is more appropriate for their experimental needs.

- **Bonsai**

Bonsai is an open-source visual programming language, which provides an easy-to-use, flexible variable environment for reactive programming, tailored for data stream processing and supporting real-time interface with different hardware devices [21]. The sound card device is implemented in Bonsai through the Harp protocol [20]. Therefore, it is possible to send commands directly from the computer to the device, including playing sounds, setting attenuation values, and others. This is the most flexible and complete control option as it exposes every single function available to the board, enables precise logging of all hardware state changes, and the ability to easily interface the presented hardware with the vast ecosystem of devices already present in Bonsai (e.g. cameras, microphones, electrophysiology, etc. . .).

- **GUI**

In addition to the generation and uploading of waveforms, the GUI can be used to send commands to the sound card. Specifically, users can play a specific sound index with configurable attenuation, with a 0.1 dB resolution attenuation for each channel.

- **External trigger**

The sound card device features a 5 V tolerant digital input that can be used to trigger a pre-selected index that contains a waveform to be played. This control strategy can be used in conjunction with either the GUI or the Bonsai to achieve reduced latency, from the trigger event to the initiation of sound.

7. Validation and characterization

7.1. Experimental validation apparatus

To fully characterize the entire signal chain and sound generation a sequential testing approach was adopted (Fig. 6). First, we characterized the performance of the sound card device (DAC). Next, we connected the audio amplifier and characterized the signal

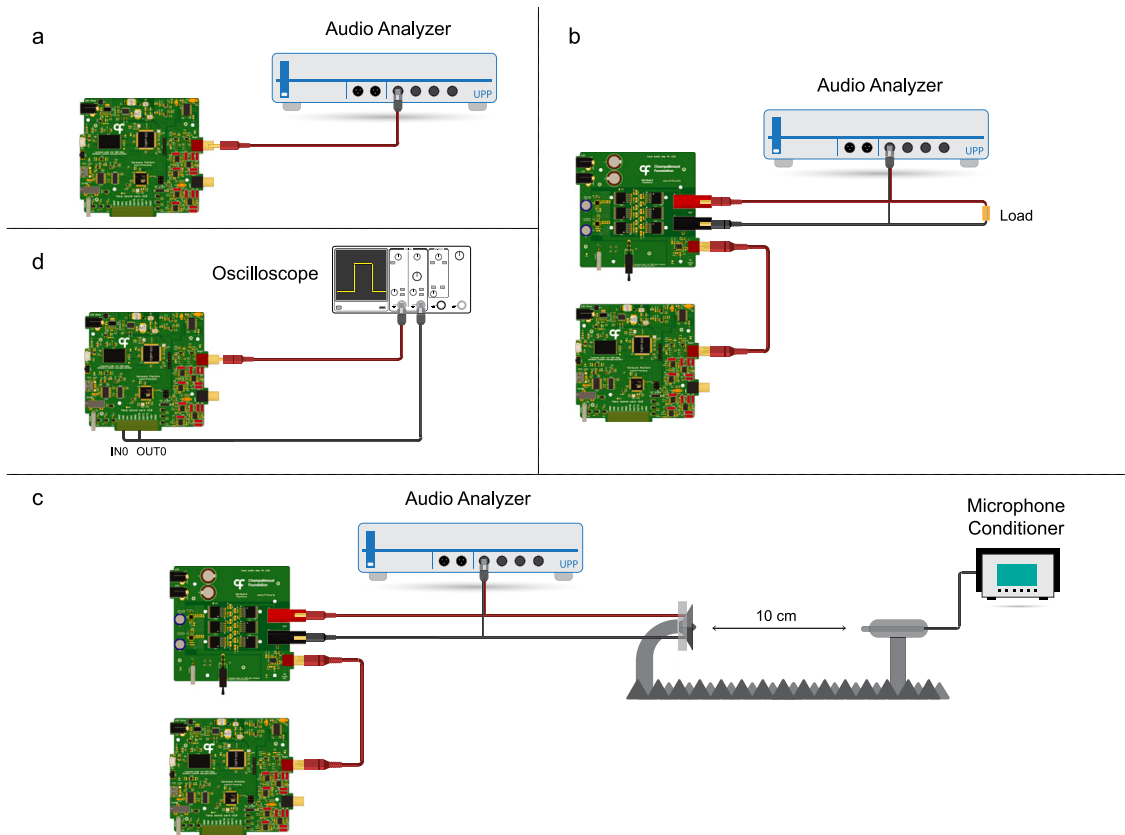


Fig. 6. Diagram of the different experimental setups used to characterize the audio system. a, Sound card device characterization setup. b, Sound card with amplifier characterization. c, Sound system with speaker frequency response using a microphone placed 10 cm away. d, Latency measurement setup.

at its output with a constant external load. Finally, we recorded the sound pressure level (SPL) response of a 4 Ω speaker connected to the output of the amplifier.

An industry-standard audio analyzer (Rohde & Schwarz UPP 400 Audio Analyzer) was used to measure and compute the audio metrics. To characterize the speaker response, a microphone connected to a conditioning amplifier (Brüel & Kjær conditioning amplifier and 4939-A-011 microphone) was used.

In addition to audio performance, we also measured the latencies associated with software and hardware-level triggering of waveform playback. All tests were performed by calculating the time difference between the trigger signal and an uploaded square waveform onset using an oscilloscope (Tektronix MSO 2004B).

7.2. Results

Waveform and sound output characterization

Given our sequential testing approach, we decided to report the following standard metrics [18] across all tests to facilitate performance comparison: Signal-to-noise (SNR) is defined as the ratio of the root mean square (RMS) signal amplitude to the mean value of the root-sum-square of all other spectral components, excluding harmonics and DC [23], meaning that only noise components are considered. SNR was measured by first determining the maximum amplitude of the output signal (6 dBV), followed by measuring the noise with a zero-input signal. The ratio between these two values corresponds to the SNR. The standalone sound card measures an SNR of 100 dB (113 dBA) (Fig. 7d), whereas the amplifier itself measures an SNR of 111 dB (119 dBA) (Fig. 9d).

The amplitude–frequency responses for both the sound card and the amplifier were measured individually (Figs. 7c and 9c). The sound card has a low pass filter with a pole at 75 kHz whereas the amplifier shows a flat response across the entire bandwidth (<0.1 dB variation over the full bandwidth).

To assess the audio distortion of the system, total harmonic distortion (THD) and total harmonic distortion plus noise (THD+N) metrics are reported. THD is defined as the ratio of the root mean square value of the fundamental signal to the mean value of the root-sum-square of its correspondent harmonics measured in the specified bandwidth [18]. In other words, THD quantifies the “purity” of the sound generated. THD+N considers also the noise components of the signal. Figs. 7e, f and 9e, f depict the frequency response of THD and THD+N, respectively, for both the standalone sound card and the sound card paired with the amplifier, using

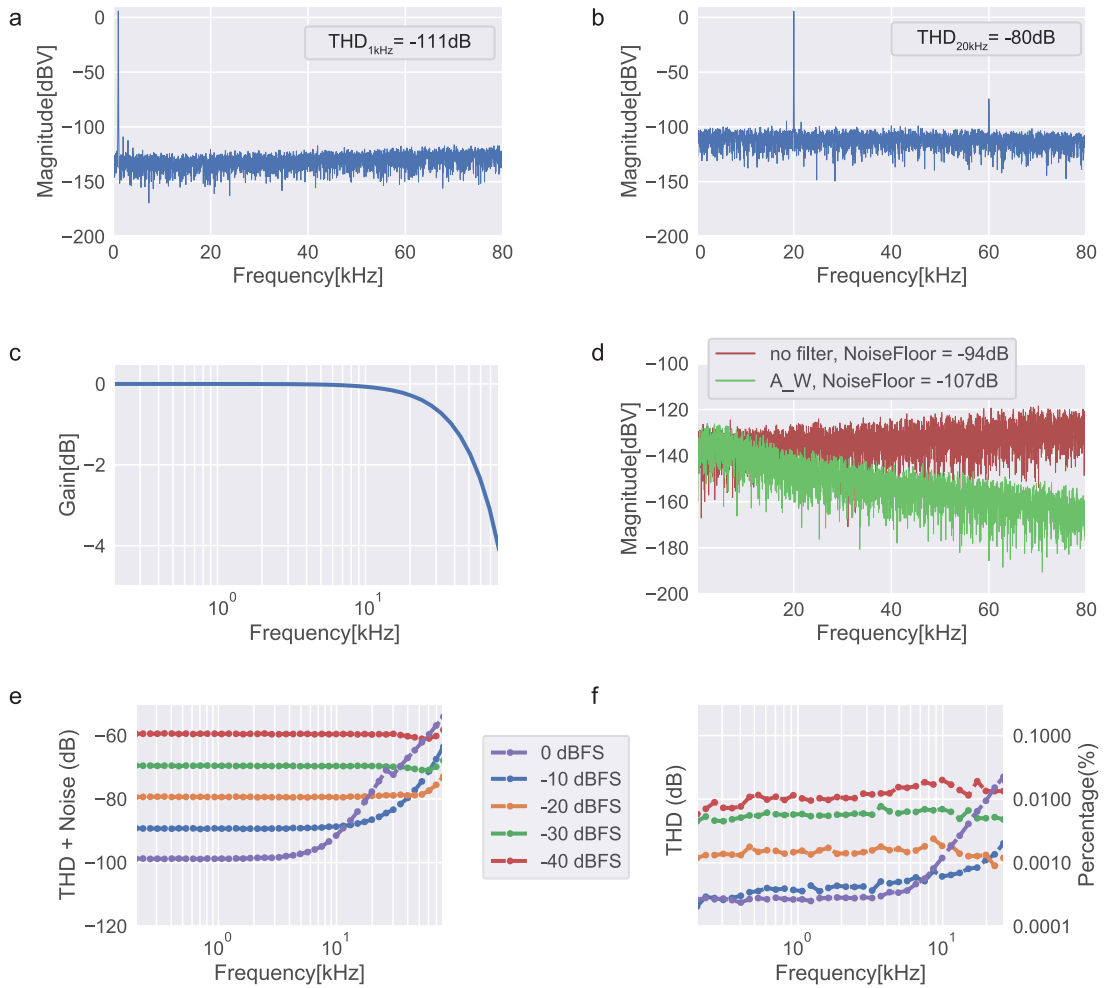


Fig. 7. Sound card output channel, configured with a 192 kHz sampling rate. a, Fast Fourier transform (FFT) for a 1 kHz sine wave signal at 0 dBFS. b, Fast Fourier transform (FFT) for a 20 kHz sine wave signal at 0 dBFS. c, Amplitude response as a function of frequency. d, Noise floor measured with zero input signal applied, with no filter and A-weighted filter for 80 kHz measuring bandwidth. e, Total harmonic distortion plus noise (THD+N) as a function of frequency for different input levels. f, Total harmonic distortion (THD) as a function of frequency for different input levels.

an external load (4Ω) across different input signal levels. A low resistance of 4Ω was chosen to induce a higher current draw, representing a worst-case scenario in terms of distortion rates in the output signals.

To summarize the response of the system across the full frequency bandwidth, we constructed a chirp signal with 1 s duration linearly sweeping up to 80 kHz, and played it through the sound card. The resulting spectrograms were captured at the output of the sound card, and then at the output of the audio amplifier when connected to the sound card under a constant load. Harmonic distortion values remained qualitatively similar between the two conditions (Fig. 8). Nonetheless, a residual distortion component relative to the second harmonic of the signal can be detected, in addition to pre-existing the 3rd harmonic distortion of the signal.

As a final test, a 4Ω speaker (Tympany XT25SC90-04) was connected to the output of the amplifier board, and a frequency response analysis was performed by generating and playing 100 distinct pure tones sweeping from 200 Hz to 80 kHz at an amplitude of -20 dBFS. A microphone connected to a conditioning amplifier (Brüel & Kjær conditioning amplifier and 4939-A-011 microphone) aligned with the speaker positioned at a 10 cm distance was used to record the SPL.

The results are depicted in Fig. 10, showing a variation response of 35 dB over the 80 kHz measuring bandwidth. It is important to note that these variations likely result from speaker-specific distortion. Nevertheless, we also show that, should a specific experiment require a flat response curve across all frequencies, a simple calibration procedure can be performed by selectively modulating the intensity of the different pure tone frequencies. Specifically, considering the magnitude of the SPL of the non-calibrated sweep, the amplitude of the 100 pure tones was adjusted to get a 70 SPL flat response. The calibrated response exhibits a variation of ± 1.1 dB over the 200 Hz - 80 kHz range.

Characterizing trigger latency

Given the tight timing often required for behavior and neurophysiological experiments, the current system affords both hardware and software triggers to instantiate a waveform playback.

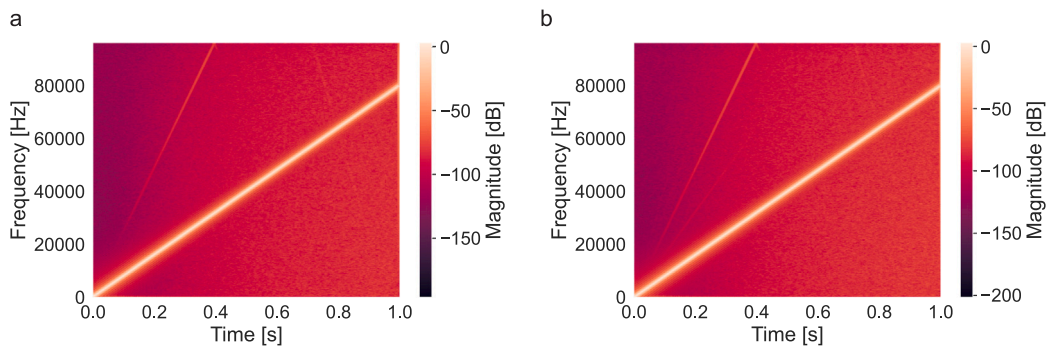


Fig. 8. Measured spectrogram based on a 0 dBFS chirp signal with 1s duration and sweep up to 80 kHz. a, Signal measured at the output of the sound card. b, Signal measured at the output of the audio amplifier connected to the sound card.

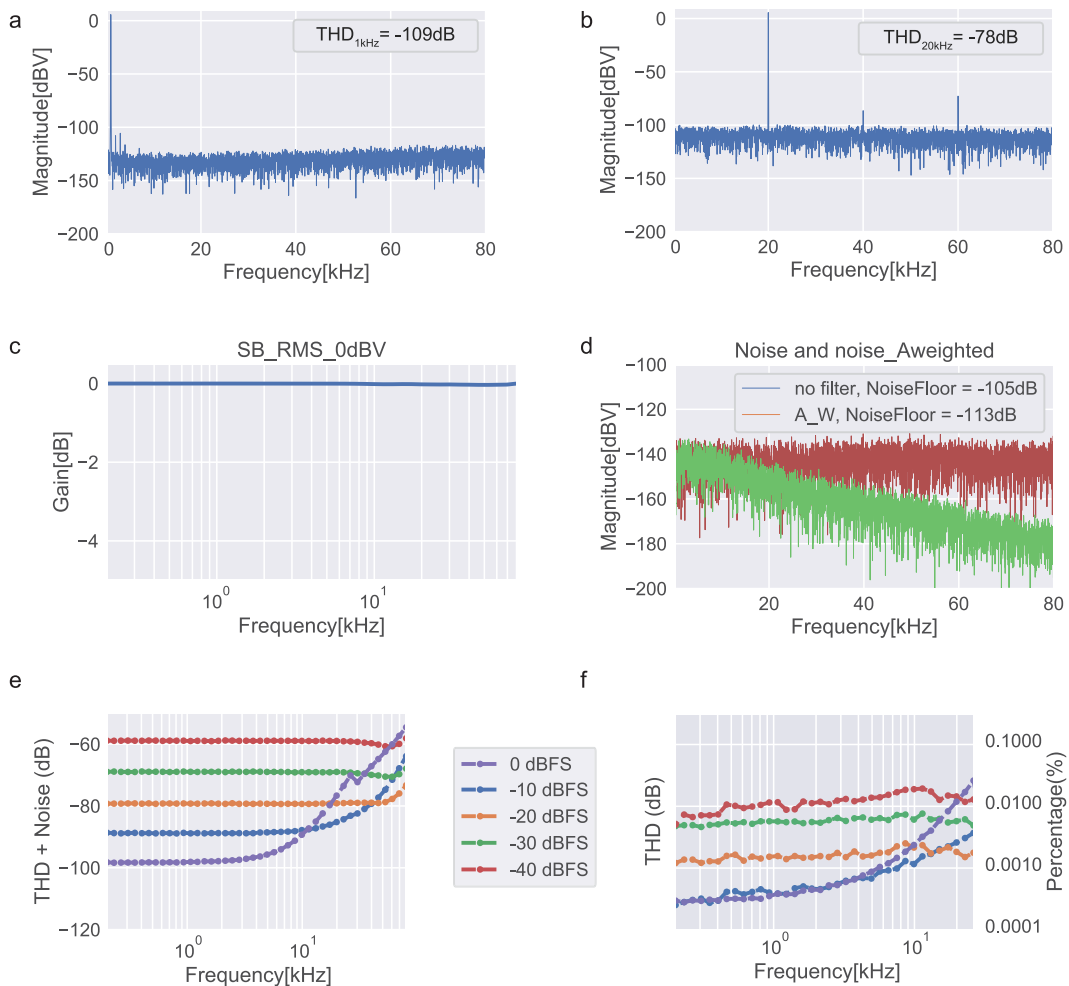


Fig. 9. Output channel of the sound card and amplifier path with a 4 Ω load, configured with a 192 kHz sampling rate. a, Fast Fourier transform (FFT) for a 1 kHz sine wave signal at 0 dBFS. b, Fast Fourier transform (FFT) for a 20 kHz sine wave signal at 0 dBFS. c, Amplifier amplitude response as a function of frequency. d, Noise floor measured with zero input signal applied, with no filter and A-weighted filter for 80 kHz measuring bandwidth (amplifier only). e, Total harmonic distortion plus noise (THD+N) as a function of frequency for different input levels. f, Total harmonic distortion (THD) as a function of frequency for different input levels.

As mentioned above, we measured the latency between an external TTL trigger and the onset of a previously uploaded square wave using the configuration illustrated in Fig. 6d. The protocol was repeated 100 times and the results are summarized in Fig. 11b.

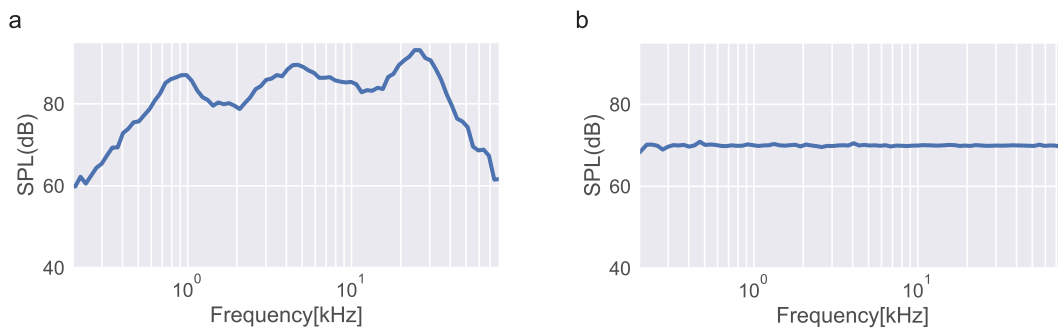


Fig. 10. Frequency response at a distance of 10 cm from a 4 Ω speaker with a -20 dBFS input signal. a, Frequency response as a function of Sound Pressure Level (SPL). b, Frequency response as a function of SPL after calibration to 70 dB.

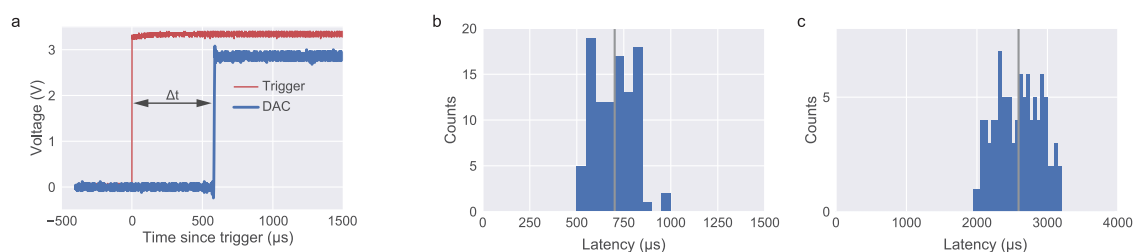


Fig. 11. Triggered playback latency. a, Trigger (blue) and generated square pulse signal (red) traces. b, Histogram for latencies measured from 100 trials with an external hardware trigger. c, Same as b, for a software trigger. See text for further details.

Table 2
Sound card device specifications.

Specification	Value
SNR	100 dB 113 dBA (20 Hz – 80 kHz @ 2 V rms)
THD	-109 dB (1 kHz @ 2 V rms)
Noise Floor	20 μ V rms -94 dB (20 Hz – 80 kHz)
Maximum sampling rate	192 kHz
Number of channels	2 channels
Number of bits	24 bits
Output Voltage	2 V rms

Table 3
Audio amplifier device specifications.

Specification	Value
SNR	111 dB 119 dBA (20 Hz – 80 kHz @ 2 V rms)
THD	-111 dB (1 kHz @ 2 V rms)
Noise Floor	5.6 μ V rms -105 dB (20 Hz – 80 kHz)
Amplitude variation over frequency	< 0.1 dB from 50 Hz to 80 kHz
Power output	4 W @ 8 Ω

Overall, all triggers resulted in a sub-millisecond latency (698 ± 104 μ s, mean \pm std), an adequate benchmark for most neuroscience behavior and neurophysiological experiments.

As an alternative, sound playback can be triggered via software. Such an option will sacrifice latency but afford users greater flexibility. Since one-way delays are notoriously difficult to calculate (as the host runs on a different clock), we opted to instead calibrate what is usually known as a round-trip delay. Briefly, a command was sent to trigger a digital output shorted to a digital input in the same board. Once the computer host received the event corresponding to this digital input toggle, a message was immediately issued to start the audio playback. The reported latency will thus correspond to the sum between the two events: “Sound card digital input event \rightarrow PC” plus “PC \rightarrow playback command”. Assuming symmetric latencies the one-way delay should be roughly the measured amount (2584 ± 313 μ s) (Fig. 11c).

Table 2 and Table 3 detail the most relevant technical specifications for the sound card and audio amplifier device, respectively.

7.3. Conclusions

In summary, the proposed audio system not only offers an open-source cost-effective alternative to commercial solutions for high-performance acoustic stimulation, especially in experiments requiring low audio distortion, but also presents a solution with reduced onset sound latency. Furthermore, this system has an extended bandwidth range of up to 80 kHz, surpassing most of the audio systems available that are designed for the human hearing frequency bandwidth range. Both the sound card and audio amplifier devices can be paired in the same audio system or used independently with other equipment.

In addition to the hardware development, a thorough characterization of the audio devices and the entire system up to the sound delivery was conducted. This is particularly important as most technical documentation for audio products relies on a limited set of flagship metrics, valid only under specific conditions, often lacking the performance analysis for a broader range of usage scenarios, namely the frequency response over the entire bandwidth or with different input signal ranges.

While fully functional, we keep maintaining and adding new features to the current system. Specifically: we intend to release a firmware update to allow single-frequency pure tones to be generated directly in firmware, without the need to upload any waveform; and a Bonsai interface update to allow the upload of arbitrary waveforms directly from Bonsai to the micro-controller.

Finally, by making all the designs open-source and with permissive licenses, we would like to encourage other developers to also contribute to the current project.

CRedit authorship contribution statement

Artur Silva: Writing – review & editing, Writing – original draft, Visualization, Validation, Methodology, Conceptualization. **Filipe Carvalho:** Writing – review & editing, Validation, Software, Methodology, Conceptualization. **Bruno F. Cruz:** Writing – review & editing, Visualization, Software, Formal analysis.

Declaration of competing interest

The authors declare the following financial interests/personal relationships which may be considered as potential competing interests: Filipe Carvalho is the director of Open Ephys Production Site.

Acknowledgments

We thank Dario Bento for assembling the boards, Mafalda Valente for providing support with the microphone-related measurements, Gonalo Lopes for help with the Bonsai interface, Alexandre Azinheira for the boards' photos, and Hugo Marques for proofreading the manuscript.

This research did not receive any specific grant from funding agencies in the public, commercial, or not-for-profit sectors.

References

- [1] Alvin Novick, Echolocation in bats: A zoologist's view, *J. Acoust. Soc. Am.* 54 (1) (1973) 139–146.
- [2] W.E. Evans, Echolocation by marine delphinids and one species of fresh-water dolphin, *J. Acoust. Soc. Am.* (1973).
- [3] Zhong Li, Jin-Xing Wei, Guang-Wei Zhang, Junxiang J Huang, Brian Zingg, Xiyue Wang, Huizhong W Tao, Li I Zhang, Corticostriatal control of defense behavior in mice induced by auditory looming cues, *Nat. Commun.* 12 (1) (2021) 1040.
- [4] Christina M. Wesolek, Gimseong Koay, Rickye S. Heffner, Henry E. Heffner, Laboratory rats (*Rattus norvegicus*) do not use binaural phase differences to localize sound, *Hear. Res.* 265 (1–2) (2010) 54–62.
- [5] Daniel E. Okobi, Jr., Arkarup Banerjee, Andrew M.M. Matheson, Steven M. Phelps, Michael A. Long, Motor cortical control of vocal interaction in neotropical singing mice, *Science* 363 (6430) (2019) 983–988.
- [6] Mafalda Valente, Juan R Castiņeiras-de Saa, Alfonso Renart, Jose L Pardo-Vazquez, Ratphones: An affordable tool for highly controlled sound presentation in freely moving rats, *Eneuro* 10 (5) (2023).
- [7] Jakob Von Uexküll, *Theoretical Biology*, Harvest Books, 1926.
- [8] Henry E. Heffner, Rickye S. Heffner, Hearing ranges of laboratory animals, *J. Am. Assoc. Lab. Animal Sci.* 46 (1) (2007) 20–22.
- [9] Alexandra Corneylie, Fabien Perrin, Lizette Heine, Sharing an open stimulation system for auditory EEG experiments using python, raspberry pi, and HifiBerry, *Eneuro* 8 (4) (2021).
- [10] N. Jeremy Hill, Scott W.J. Mooney, Glen T. Prusky, Audiomath: A neuroscientist's sound toolkit, *Heliyon* 7 (2) (2021).
- [11] Luca Vignati, Stefano Zambon, Luca Turchet, A comparison of real-time linux-based architectures for embedded musical applications, *J. Audio Eng. Soc.* 70 (1/2) (2022) 83–93.
- [12] Eduardo Meneses, Johnty Wang, Sergio Freire, Marcelo M Wanderley, A comparison of open-source linux frameworks for an augmented musical instrument implementation, in: *NIME*, 2019, pp. 222–227.
- [13] Luca Turchet, Carlo Fischione, Elk audio OS: an open source operating system for the internet of musical things, *ACM Trans. Internet Things* 2 (2) (2021) 1–18.
- [14] Andrew McPherson, Victor Zappi, An environment for submillisecond-latency audio and sensor processing on BeagleBone black, in: *Audio Engineering Society Convention 138*, Audio Engineering Society, 2015.
- [15] Henrik Langer, Robert Manzke, Embedded multichannel linux audiosystem for musical applications, in: *Proceedings of the 12th International Audio Mostly Conference on Augmented and Participatory Sound and Music Experiences*, 2017, pp. 1–5.
- [16] Sanworks, https://sanworks.github.io/Bpod_Wiki/assembly/hifi-module-assembly/.
- [17] Gloria G Parras, Javier Nieto-Diego, Guillermo V Carbajal, Catalina Valdés-Baizabal, Carles Escera, Manuel S Malmierca, Neurons along the auditory pathway exhibit a hierarchical organization of prediction error, *Nat. Commun.* 8 (1) (2017) 2148.
- [18] Michael Lohse, Johannes C Dahmen, Victoria M Bajo, Andrew J King, Subcortical circuits mediate communication between primary sensory cortical areas in mice, *Nature Commun.* 12 (1) (2021) 3916.

- [19] Stitipragyan Bhumika, Mari Nakamura, Patricia Valerio, Magdalena Solyga, Henrik Lindén, Tania R Barkat, A late critical period for frequency modulated sweeps in the mouse auditory system, *Cerebral Cortex* 30 (4) (2020) 2586–2599.
- [20] **harp-tech**, <https://github.com/harp-tech/protocol>.
- [21] Gonçalo Lopes, Niccolò Bonacchi, João Frazão, Joana P Neto, Bassam V Atallah, Sofia Soares, Luís Moreira, Sara Matias, Pavel M Itskov, Patrícia A Correia, et al., Bonsai: An event-based framework for processing and controlling data streams, *Front. Neuroinform.* 9 (2015) 7.
- [22] Thomas Akam, Andy Lustig, James M Rowland, Sampath KT Kapaniaiah, Joan Esteve-Agraz, Mariangela Panniello, Cristina Márquez, Michael M Kohl, Dennis Kätzel, Rui M Costa, et al., Open-source, python-based, hardware and software for controlling behavioural neuroscience experiments, *ELife* 11 (2022) e67846.
- [23] Walt Kester, *Mixed-Signal and DSP Design Techniques*, Newnes, 2003.



Artur Silva holds a M.Sc. degree in Computer and Electrical Engineering with specialization in Electronics. He works in hardware development targeted for different research domains and is an active contributor of open source projects.



Filipe Carvalho holds a Master of Science degree in Computer and Electrical Engineering. He actively contributes with electronic designs to various projects around the globe, advocating for open-source principles. He is the founder of the Open Ephys Production Site and collaborator on NeuroGEARS.